

1 **Pacing Early Mars fluvial activity at Aeolis Dorsa: Implications for Mars**  
2 **Science Laboratory observations at Gale Crater and Aeolis Mons**

3

4 Edwin S. Kite<sup>a</sup> (ekite@caltech.edu), Antoine Lucas<sup>a</sup>, Caleb I. Fassett<sup>b</sup>

5 <sup>a</sup> Caltech, Division of Geological and Planetary Sciences, Pasadena, CA 91125

6 <sup>b</sup> Mount Holyoke College, Department of Astronomy, South Hadley, MA 01075

7

8 **Abstract:** The impactor flux early in Mars history was much higher than today, so sedimentary  
9 sequences include many buried craters. In combination with models for the impactor flux,  
10 observations of the number of buried craters can constrain sedimentation rates. Using the  
11 frequency of crater-river interactions, we find net sedimentation rate  $\lesssim 20\text{-}300 \mu\text{m}/\text{yr}$  at Aeolis  
12 Dorsa. This sets a lower bound of 1-15 Myr on the total interval spanned by fluvial activity  
13 around the Noachian-Hesperian transition. We predict that Gale Crater's mound (Aeolis Mons)  
14 took at least 10-100 Myr to accumulate, which is testable by the Mars Science Laboratory.

15

16 **1. Introduction.**

17 On Mars, many craters are embedded within sedimentary sequences, leading to the  
18 recognition that the planet's geological history is recorded in "cratered volumes", rather than  
19 just cratered surfaces (Edgett and Malin, 2002). For a given impact flux, the density of craters  
20 interbedded within a geologic unit is inversely proportional to the deposition rate of that  
21 geologic unit (Smith et al. 2008). To use embedded-crater statistics to constrain deposition  
22 rate, it is necessary to distinguish the population of interbedded craters from a (usually much  
23 more numerous) population of craters formed during and after exhumation. However, on  
24 Mars, erosion can exhume intact impact craters complete with ejecta blankets from beneath  
25 hundreds of meters of overlying sediment (e.g., Edgett, 2005). Variations in burial, exhumation,

26 viscous relaxation, and erosion produce varying crater-preservation styles (Figure 1). Because  
27 of the difficulty of determining which craters are syndepositional, we do not know of any  
28 previous measurements of fluvial sedimentation rates on Mars using the frequency of  
29 embedded impact craters.

30 Geological evidence suggests a period of enhanced precipitation-fed fluvial erosion created  
31 regionally-integrated highland valley networks around the Noachian-Hesperian boundary  
32 ~3.6-3.7 Ga (Irwin et al., 2005). Regionally-integrated fluvial activity ceased planetwide at  
33 roughly the same time, perhaps even synchronously (Fassett et al., 2011), although limited  
34 and/or localized fluvial activity continued afterward (e.g., Grant & Wilson, 2011; Mangold et al.,  
35 2012). Lake-basin hydrology disfavors valley-network formation by a single deluge (Barnhart  
36 et al., 2009; Matsubara et al., 2011). Improved constraints on the pace and persistence of  
37 fluvial activity during the Noachian-Hesperian transition are required to understand early  
38 Mars climate and habitability. It remains unclear whether the fluvial geomorphology of the  
39 Noachian-Hesperian transition is a palimpsest of transient events triggered by volcanic  
40 eruptions or impacts (Segura et al., 2008; Kite et al., 2011; Wordsworth et al., 2012), or  
41 alternatively records a sustained ( $\gg 1$  Kyr) wet interval(s) caused by unusual orbital  
42 conditions (Kite et al., 2012a), an early greenhouse (Sagan & Mullen, 1972), or an impact-  
43 triggered excursion to a warm stable state (Segura et al., 2012).

44 Here we use interactions between craters and fluvial deposits to determine sedimentation  
45 rate within a Late Noachian/Early Hesperian sedimentary basin containing numerous fluvial  
46 deposits. A river flowing over a heavily cratered sedimentary landscape will be frequently  
47 diverted by crater rims and/or deposit sediment in pools corresponding to the crater interiors  
48 (Figure 1). These craters, and craters partly overlain by river deposits, are readily identified as  
49 being syndepositional.

50

51 **2. River-crater interactions.**

52 We search for river-crater interactions within exceptionally numerous and well-preserved  
53 fluvial channel deposits exhumed by erosion in the Aeolis Dorsa region, formerly termed  
54 Aeolis-Zephyria Planum (Burr et al., 2009, 2010; note that we use Aeolis Dorsa to refer to the  
55 formally defined region, not just the ridges within that region). The area of our search (~6S,  
56 152E; Figure 2) is stratigraphically ~500m below a surface with an Early Hesperian, minimum  
57 model age of  $3.69(+0.05/-0.07)$  Ga (Zimbelman & Scheidt, 2012, using the Ivanov et al., 2001  
58 production function and the Hartmann & Neukum, 2001 chronology function). It forms part of  
59 an eroded deposit that is thought to be Late Noachian or Early Hesperian (Irwin et al., 2004).  
60 These dates correlate the Aeolis rivers to the Noachian-Hesperian transition and to the lower  
61 Gale Crater mound (Fassett & Head, 2008; Kerber & Head, 2010; Thomson et al, 2011;  
62 Zimbelman & Scheidt, 2012); they allow for the rivers to either predate, or correlate with, the  
63 lower Gale Crater mound.

64 Packing density of channel deposits within the stratigraphy is comparable to Earth  
65 fluviodeltaic basins (e.g., Gouw, 2008). The Martian rivers are qualitatively similar to  
66 meandering-river deposits on Earth. Interactions with craters are, therefore, easily recognized  
67 as anomalous. Impact craters are identified by random distribution across the landscape,  
68 obliteration of older geological structures within the transient cavity, and especially circularity  
69 and upturned rims. Interfluvial material would be interpreted as the fine-grained deposits of  
70 rare floods if this were a basin on Earth. However, in the absence of grain-size data or  
71 diagnostic levee-breach features, wind-blown dust and silt cannot be ruled out (Haberlah et al.,  
72 2010). From local relationships the stratigraphic thickness of deposits containing fluvial  
73 channels,  $\Delta z$ , is  $> 100$ m. Channel deposits are exposed over a ~1km elevation range, but  
74 postdepositional modification complicates reconstruction of  $\Delta z$  (Lefort et al., 2012). A likely

75 lower bound on  $\Delta z$  is the difference between the modern surface and a surface interpolated  
76 inward from low points surrounding the fluvial region. This gives  $\Delta z \gtrsim 300\text{m}$ .

77 17 exhumed craters are found (Supplementary Table) at multiple stratigraphic levels  
78 within  $2100\text{ km}^2$  of fluvial deposits surveyed with CTX images (5-6 m/pixel). Identifications  
79 were checked where possible with higher-resolution images (HiRISE or MOC). In addition to  
80 these features that are definitely identified as embedded within the stratigraphy and having  
81 definite impact crater morphology, an additional 43 candidates were found. Crater diameters  
82 were obtained by fitting a circle to the visible arc of the crater edge. Embedded-crater size-  
83 frequency distributions for  $D > 250\text{m}$  ( $D$  is diameter) have a cumulative power-law slope  
84 slightly shallower than  $-2$ ,  $\sim 1$  less than the production-function slope of  $-3$  in this range. This  
85 is expected for a crater population embedded within a volume (Yielding et al., 1996); a pristine  
86 crater population on a geologically stable surface would parallel the production function.  
87 Craters  $D \lesssim 250\text{ m}$  are still further underrepresented, which we interpret as the result of  
88 survey incompleteness or poor exhumed-crater preservation at small sizes.

89

### 90 **3. Constraints on sedimentation rate and fluvial timescales.**

91 We make the following initial assumptions –

92 (i) Cratering is a Poisson process with an initial crater depth,  $d \approx 0.2D$  for  $D < 1\text{km}$  (Melosh,  
93 1989).

94 (ii) Erosion does not preferentially expose craters.

95 (iii) During deflation of the deposit an embedded crater is invisible until the deflation  
96 surface reaches the embedded-crater rim. It is then visible at its original diameter until the  
97 deflation surface reaches the level of the bottom of the crater.

98 We discuss possible violations of these assumptions later.



99 The flux of impact craters at the time the deposit was forming,  $f(D>D_i)$ , is obtained  
100 using the crater-production and crater-chronology functions recommended by Werner &  
101 Tanaka (2011). Differences between the Hartmann and Ivanov/Neukum-Hartmann functions  
102 lead to <20% disagreement in resurfacing rate for the size-range of craters used here (Figure  
103 3), which is unimportant compared to other uncertainties. The expected number of embedded  
104 craters,  $N_{cr}$ , is given by

$$105 \quad N_{cr}(D>D_i) = f(D>D_i) (d/D) D a / S$$

106 where  $a$  is count area, and  $S$  is accumulation rate. Excluding  $D < 290\text{m}$  craters and assuming an  
107 age in the range 3.7 – 3.9 Ga, least-squares fitting of accumulation rates to the data (Figure 3)  
108 gives  $S = 20\text{-}80 \mu\text{m/yr}$  (or  $70\text{-}300 \mu\text{m/yr}$  including all candidates). Therefore,  $S \approx 20\text{-}300$   
109  $\mu\text{m/yr}$  for the range of likely ages.

110 The most important uncertainty is  $f$ . The Aeolis Dorsa river deposits were emplaced during  
111 a period of higher crater flux  $f$  when rapid changes in  $f$  are also possible, potentially associated  
112 with the Late Heavy Bombardment. Therefore, small changes in the age of the deposit may lead  
113 to large changes in  $S$  (Werner & Tanaka, 2011). Crater-chronology functions are defined based  
114 on the lunar sample collection, whose interpretation is somewhat model-dependent, and the  
115 translation of these data to Mars is challenging (e.g., Ivanov, 2001).

116 Other uncertainties tend to lead to an underestimate of exhumed-crater frequency. (a) If  
117 channel belts aggraded faster than interfluves and are erosionally resistant, and erosion is by  
118 vertical downcutting uncorrelated with laterally adjacent terrain, then at any given time the  
119 modern deflation surface will preferentially expose the erosion-resistant, crater-deficient  
120 units. In this case our procedure would underestimate the frequency of craters per unit volume  
121 averaged over the basin. On Earth, channel belts always aggrade faster than their floodplains  
122 on interannual timescales, but levee breaches and avulsions maintain constant aggradation  
123 rate across the floodplain averaged over depths greater than  $\sim 1$  channel depth (Mohrig et al.,

124 2000). Channel-width measurements (Burr et al., 2010), standard fluvial scaling relations, and  
125 HiRISE DTM measurements of negative-relief channel depths indicate that Aeolis channel  
126 depths should be small compared to the original depth of the craters in our count (i.e. channel  
127 depth  $\ll$  30-60m). Therefore lateral gradients in sedimentation rate are unlikely to be  
128 important if the interfluves are floodplain deposits. (b) Cliff-forming units that are very  
129 resistant to vertical abrasion will be removed by lateral mass wasting as surrounding weaker  
130 material is eroded. In this case, no embedded craters within the cliff-forming unit will be  
131 included in the count: craters on top of the cliff-forming unit will be hard to distinguish from  
132 relatively recent synerosional craters, and craters within the unit will be blanketed by talus  
133 throughout the erosion process. The effective count area then scales with the perimeter of the  
134 cliff-forming unit, rather than with its area. (c)  $S$  would halve in the extreme case that all  
135 craters initially have a secondary-like  $d/D$  (i.e.,  $\sim 0.1$ ).  $d/D$  is currently  $< 0.1$  in our HiRISE  
136 DTMs, but this could be due to incomplete erosion or recent infilling. (d) Supposing small  
137 craters were all erosionally resistant and formed mesas as tall as their diameter, assumption  
138 (iii) would be violated and a surface count would overestimate the true crater density.  
139 However, our CTX and HiRISE DTMs show that small exhumed craters are not locally  
140 highstanding in this region, although they do tend to be preserved with rims intact, so (iii) is  
141 probably a good approximation. (e) We assume craters are either present at full diameter or  
142 eliminated completely. (f) Finally, we neglect possible erosion of craters *during* the period of  
143 net accumulation.

144       Because these errors tend to lead to an undercount of the number of craters that formed  
145 during the interval of fluvial deposition, we interpret our data as a lower limit on time for  
146 accumulation. Assuming  $\Delta z \gtrsim 300\text{m}$ , the range of minimum deposition timescale is  $\Delta z/S \sim 1\text{-}15$   
147 Ma for the range of likely ages (or 0.5-30 Ma assuming a wider range of age uncertainty, from  
148 3.6-4.0 Ga).

149 **4. Discussion.**

150 The simplest interpretation of these data is fluvial aggradation at rates comparable to Earth  
151 (fluvial aggradation rates ranging from 50-600  $\mu\text{m}/\text{yr}$  are compiled by Miall, 2012). Aeolis  
152 Dorsa sedimentation cannot be distinguished from later sedimentation on the basis of  
153 sedimentation rate alone. Putzig et al. (2009) correlate radar reflectors within the North Polar  
154 Layered Deposits to 0-4 Mya obliquity cycles and obtain  $S \sim 1$  mm water ice/yr. Similarly,  
155 Lewis et al. (2008) correlate bed:bundle ratios in Becquerel Crater at 22°N to Milankovitch  
156 beats and obtain  $S \sim 30$   $\mu\text{m}/\text{yr}$ . Typical equatorial mound rhythmic-layer thicknesses of 3-20m  
157 (Lewis et al., 2010) imply accumulation at 20-200  $\mu\text{m}/\text{yr}$  if forced by obliquity cycles (0.12  
158 Myr), or 100-800  $\mu\text{m}/\text{yr}$  if forced by precession (0.025 Myr effective period at the equator).  
159 Rhythmites have been hypothesized to be relatively young (Grotzinger & Milliken, in press).  
160 Modern gross sedimentation rate on Mars is 10-100  $\mu\text{m}/\text{year}$  from dust storms (Drube et al.,  
161 2010).

162 On Earth, mean sedimentation rate frequently decreases with increasing measurement  
163 duration (Jerolmack & Sadler, 2007) as a result of power-law fluctuations of the boundary  
164 between erosion and deposition (Schumer & Jerolmack, 2009). This “Sadler effect” is  
165 ubiquitous at short timescales near coasts but is less relevant on the longest timescales, or  
166 where erosion is unimportant (Jerolmack & Sadler, 2007). It is not clear whether the Sadler  
167 effect should apply to Mars sediments. Martian weather is remarkably predictable on both  
168 synoptic and interannual timescales, probably because of the lack of a large energy capacitor  
169 analogous to Earth’s ocean (Read & Lewis, 2004). Therefore, we might speculate that Mars’  
170 sedimentary record, as the imprint of the atmosphere on rocks, is less chaotic than its Earth  
171 counterpart. Consistent with this, quasi-periodic bedding is common on Mars (Lewis et al.,  
172 2010) and angular unconformities are rare. Our data hint that exhumed craters are  
173 concentrated at a few stratigraphic levels, consistent with omission surfaces.

174 The sediment source for the Aeolis Dorsa deposits is uncertain. It is possible that sediment  
175 was fluviably transported from highlands to the south. However, the volume of valley networks  
176 draining toward Aeolis Dorsa appears to be much smaller than the volume of the clastic wedge,  
177 and no complete transport pathways are visible. It is conceivable that the Aeolis Dorsa deposits  
178 are fluviably reworked ancient highlands crust, which would require that the dichotomy  
179 boundary was once further to the north. But crater-floor tilts suggest that the dichotomy  
180 boundary was in place near its current location prior to the late Noachian (Watters et al.,  
181 2007). An attractive possibility is that the fluvial deposits are reworked from relatively weak  
182 aeolian or niveoaeolian deposits accumulating at the highland-lowland boundary (Irwin,  
183 2004).

184 The relatively low embedded-crater frequency is in line with low Platinum Group Element  
185 concentrations in 3.8 Ga metasediments from Earth (Anbar et al., 2001).

186

## 187 **5. Implications for ancient climate and MSL's mission to Gale Crater.**

188 A lower bound of 1-15 Myr for the total interval spanned by fluvial deposition rules out basin-  
189 filling by a single catastrophic episode, and is consistent with hydrologic and total-erosion  
190 estimates for fluvial activity around the Noachian-Hesperian boundary (Barnhart et al., 2009;  
191 Hoke et al., 2011). Possible climate regimes include multiple climate transients (Segura et al.  
192 2008, Wordsworth et al. 2012), or intermittent precipitation-fed runoff over  $\geq 10^5$  yr (Barnhart  
193 et al., 2009). The implied total time interval recorded by Gale-Aeolis sediments is  $\geq 10^{7-8}$  yr.  
194 The sedimentary rock record of Mars appears to record a small fraction of Mars history,  
195 perhaps because surface liquid water was necessary for lithification and was only available  
196 intermittently (the wet-pass filter hypothesis; Moore, 1990, Knoll et al., 2008, Andrews-Hanna  
197 & Lewis, 2011, Kite et al., 2012a).

198 Based on observed and candidate embedded-crater frequency in Aeolis Dorsa, we predict a  
199 mean Aeolis Mons sedimentation rate of 20-300  $\mu\text{m}/\text{yr}$  including nondepositional intervals.  
200 This is testable with MSL measurements of cosmogenic noble gases (e.g., Shuster et al., 2012),  
201 meteoritic Ni (Yen et al., 2006), meteoritic organic matter (OM), and small embedded craters.  
202 Mars Hand Lens Imager's (MAHLI's) 14 $\mu\text{m}$  resolution permits identification of  $\geq 50\mu\text{m}$ -thick  
203 varves, if they exist.

204 Sediment accumulation rate affects the rate at which OM from meteoritic infall is  
205 introduced to the record – the “meteoritic background level” (Summons et al., 2011).  
206 Preservation of OM introduced at the surface is affected by time-to-burial to a depth of order  
207 1m. During this time, OM is vulnerable to degradation by radiation, atmospheric oxidants,  
208 and/or UV, to an extent that depends on the unknown redox state, composition and thickness  
209 of Early Mars' atmosphere (Pavlov et al., 2012). On Earth, overbank environments and oxbow  
210 lakes in meander belts are favored among subaerial environments for preserving organic  
211 matter (Summons et al., 2011).

212 River deposits exist at the Gale mound, but those clearly identifiable from orbit appear to  
213 postdate the accumulation of the lower unit of Aeolis Mons. It has been argued that the  
214 primary sediment source for the Gale mound is airfall (Pelkey et al., 2004; Thomson et al.,  
215 2011; Kite et al., 2012b). If this is true, then the extrapolation of the Aeolis Dorsa  
216 sedimentation rate to Aeolis Mons depends on the assumption that river sediment was  
217 supplied by aeolian processes (e.g., Irwin et al., 2004; Haberlah, 2010).

218 Future work might use MSL data to assess the relation between exposure time, crater  
219 frequency, OM preservation, and atmospheric paleopressure. The existence of  $>3.7$  Gya,  
220  $\leq 10^2\text{m}$ -diameter craters should place an upper limit on ancient atmospheric pressure (Popova  
221 et al., 2003); we are pursuing this quantitatively.

222

223 **Acknowledgements:** We thank Mike Lamb, Ken Farley, Lauren Edgar, Katie Stack, Mathieu  
224 Lapôtre, Roman DiBiase, Kirsten Siebach, Ken Farley, Joel Schiengross, Devon Burr, Alexandra  
225 Lefort, Robert Jacobsen, and especially Mark Allen, Woody Fischer, Kevin Lewis, and Nick  
226 Warner, for discussions. We additionally thank Kevin Lewis and Oded Aharonson for sharing  
227 their preprint on cyclic bedding (which was referred to extensively in writing this paper), Oded  
228 Aharonson for comments that significantly improved the manuscript, and Mark Allen for  
229 reminding us of the importance of resurfacing rate to organic-matter preservation. We  
230 thank the HiRISE team for maintaining a responsive public target request program, HiWish,  
231 which was useful for this work. DTMs produced for this work,  
232 ESP\_17548\_1740/ESP\_019104\_1740 (@1m/pixel) and PSP\_007474\_1745/ ESP\_024497\_1745  
233 (@2.5m/pixel) are available for unrestricted further use from the corresponding author.

234

235 **References:**

236 Anbar, A.D., et al., 2001, Extraterrestrial iridium, sediment accumulation and the habitability of  
237 the early Earth's surface. *J. Geophys. Res.*, 106, 3219-3236.

238 Andrews-Hanna, J.C. & Lewis, K.W., 2011, Early Mars hydrology: 2. Hydrological evolution in  
239 the Noachian and Hesperian epochs. *J. Geophys. Res.* 116, E02007.

240 Barnhart, C.J. et al., 2009, Long-term precipitation and late-stage valley network formation:  
241 Landform simulations of Parana Basin, Mars. *J. Geophys. Res.*, 114, E01003.

242 Burr, D.M., et al., 2009, Pervasive aqueous paleoflow features in the Aeolis/Zephyria Plana  
243 region, Mars. *Icarus*, 200, 52-76.

244 Burr, D. M., et al., 2010, Inverted fluvial features in the Aeolis/Zephyria Plana region, Mars:  
245 Formation mechanism and initial paleodischarge estimates. *J. Geophys. Res.*, 115, E07011.

246 Drube, L., et al., 2010, Magnetic and optical properties of airborne dust and settling rates of  
247 dust at the Phoenix landing site. *J. Geophys. Res.*, 115, E00E23.

248 Edgett, K.S., 2005, The sedimentary rocks of Sinus Meridiani, *Mars Journal*, 1, 5-58.

249 Edgett, K. S., & Malin, M. C., 2002. Martian sedimentary rock stratigraphy, *Geophys. Res. Lett.*,  
250 29, 2179.

251 Fassett, C.I., & Head, J. W. , 2008, The timing of martian valley network activity: Constraints  
252 from buffered crater counting. *Icarus*, 195, 61-89.

253 Fassett, C. I., & Head., J. W., 2011, Sequence and timing of conditions on early Mars. *Icarus*, 211,  
254 1204-1214.

255 Grant, J. A., & Wilson, S. A., 2011, Late alluvial fan formation in southern Margaritifer Terra,  
256 *Mars. Geophys. Res. Lett.*, 380:L08201.

257 Grotzinger, J.P., & Milliken, R.E., in press, The sedimentary rock record of Mars, p. 1-48 *in*  
258 *Sedimentary Geology of Mars*, SEPM Special Publication no. 11.

259 Gouw, M.J. P., 2008, Alluvial architecture of the Holocene Rhine-Meuse delta. *Sedimentology*,  
260 55, 1487.

261 Haberlah, D., et al., 2010, Loess and floods: High-resolution multi-proxy data of Last Glacial  
262 Maximum (LGM) slackwater deposition in the Flinders Ranges, semi-arid South Australia. *Quat.*  
263 *Sci. Rev.*, 29, 2673-2693.

264 Hartmann, W.K. & Neukum, G., 2001, Cratering Chronology and the Evolution of Mars. *Space*  
265 *Sci. Rev.*, 96, 165-194.

266 Hoke, M.R.T., et al. 2011, Formation timescales of large Martian valley networks. *Earth Planet.*  
267 *Sci. Lett.*, 312, 1-12.

268 Irwin, R.P., et al., J.R., 2004, Sedimentary resurfacing and fretted terrain development along the  
269 crustal dichotomy boundary, Aeolis Mensae, *Mars. J. Geophys. Res.*, 109, E09011.

270 Irwin, R.P. III, et al., 2005, An intense terminal epoch of widespread fluvial activity on early  
271 Mars: 2. Increased runoff and paleolake development. *J. Geophys. Res.* 110, E12S15.

272 Ivanov, B.A., 2001, Mars/Moon Cratering Rate Ratio Estimates. *Space Sci. Rev.*, 96, 87.

273 Jerolmack, D.J. & Sadler, P., 2007, Transience and persistence in the depositional record of  
274 continental margins. *J. Geophys. Res.*, 112, F03S13.

275 Kerber, L. & Head, J.W., 2010, The age of the Medusae Fossae Formation, *Icarus*, 206, 669.

276 Kite, E.S., et al. 2011, Localized precipitation and runoff on Mars. *J. Geophys. Res.* 116, E07002.

277 Kite, E.S., et al., 2012a, Seasonal melting and the formation of sedimentary rocks on Mars, with  
278 predictions for the Gale Crater mound, submitted to *Icarus*, astro-ph:EP, arXiv:1205.6226.

279 Kite, E.S., et al., 2012b, Growth and form of the mound in Gale Crater, Mars: Slope-wind  
280 enhanced erosion and transport, astro-ph:EP, arXiv:1205.6840.

281 Knoll, A.H., et al., 2008, Veneers, rinds, and fracture fills: Relatively late alteration of  
282 sedimentary rocks at Meridiani Planum, Mars. *J. Geophys. Res.*, 113(E6), E06S16.

283 Lewis, K.W., et al., 2008, Quasi-periodic bedding in the sedimentary rock record of Mars.  
284 *Science*, 322, 1532.

285 Lewis, K.W., et al., 2010, *Lunar Planet Sci. Conf.* 41, abstract # 2648.

286 Matsubara, Y. et al. 2011, Hydrology of early Mars: Lake basins. *J. Geophys. Res.*, 116, E04001.

287 Lefort, A., et al., 2012, Inverted fluvial features in the Aeolis-Zephyria Plana, western Medusae  
288 Fossae Formation, Mars: Evidence for post-formation modification. *J. Geophys. Res.*, 117,  
289 E03007.

290 Mangold, N., et al., 2012, The origin and timing of fluvial activity at Eberswalde crater, Mars.  
291 *Icarus*, 220, 231-251.

292 Melosh, H. J. 1989. *Impact cratering: a geologic process*. New York: Oxford University Press.

293 Miall, A.D., 2012, A new uniformitarianism: stratigraphy as just a set of “frozen accidents,”  
294 preprint, [http://www.geology.utoronto.ca/Members/miall/miall\\_bib/pdfs/Miall2012.pdf/](http://www.geology.utoronto.ca/Members/miall/miall_bib/pdfs/Miall2012.pdf/).

295 Mohrig, D., et al., 2000, Interpreting avulsion process from ancient alluvial sequences:  
296 Guadalupe-Matarranya system (northern Spain) and Wasatch formation (western Colorado).  
297 *Geol. Soc. Am. Bull.*, 112, 1787 – 1803.



298 Moore, J.M., 1990, Nature of the mantling deposit in the heavily cratered terrain of  
299 northeastern Arabia, Mars. *J. Geophys. Res.*, 95, 14279-14289.

300 Pelkey, S.M., et al., 2004 Surficial properties in Gale Crater, Mars, from Mars Odyssey THEMIS  
301 data. *Icarus*, 167, 244-270.

302 Popova, O., et al., 2003, Bolides in the present and past Martian atmosphere and effects on  
303 cratering processes. *Meteoritics and Planetary Science*, 38, 905-925.

304 Putzig, N., et al., 2009, Subsurface structure of Planum Boreum from Mars Reconnaissance  
305 Orbiter Shallow Radar soundings, *Icarus*, 204, 443-457.

306 Read, P.L., & S.R. Lewis, 2004, *The Martian Climate Revisited: Atmosphere and Environment of  
307 a Desert Planet*, Springer-Praxis.

308 Sagan, C., & Mullen, G., 1972, Earth and Mars: Evolution of atmospheres and surface  
309 temperatures. *Science*, 177, 52-56.

310 Schumer, R., & Jerolmack, J.D., 2009, Real and apparent changes in sediment deposition rates  
311 through time, *J. Geophys. Res.* 114, F00A06.

312 Segura, T.L., et al., 2008, Modeling the environmental effects of moderate-sized impacts on  
313 Mars. *J. Geophys. Res.*, 113, E11007.

314 Segura, T.L., et al., 2012, An impact-induced, stable, runaway climate on Mars. *Icarus*, 220, 144.

315 Shuster, D.L., et al., 2012, Cosmogenic <sup>3</sup>He in hematite and goethite from Brazilian “canga”  
316 duricrust demonstrates the extreme stability of these surfaces. *Earth Planet. Sci. Lett.*, 329, 41.

317 Smith, M.R., et al., 2008, Effect of obliteration on crater-count chronologies for Martian  
318 surfaces, *Geophys. Res. Lett.*, 35, L10202.

319 Summons, R.E., et al., 2011, Preservation of Martian Organic and Environmental Records.  
320 *Astrobiology*, 11, 157-181.

321 Thomson, B.J., et al., 2011, Constraints on the origin and evolution of the layered mound in Gale  
322 Crater, Mars using Mars Reconnaissance Orbiter data. *Icarus*, 214, 413-432.

323 Watters, T.R., et al., 2007, Hemispheres apart: The crustal dichotomy on Mars. *Ann. Rev. Earth*  
324 *Planet. Sci.*, 35, 621-652.

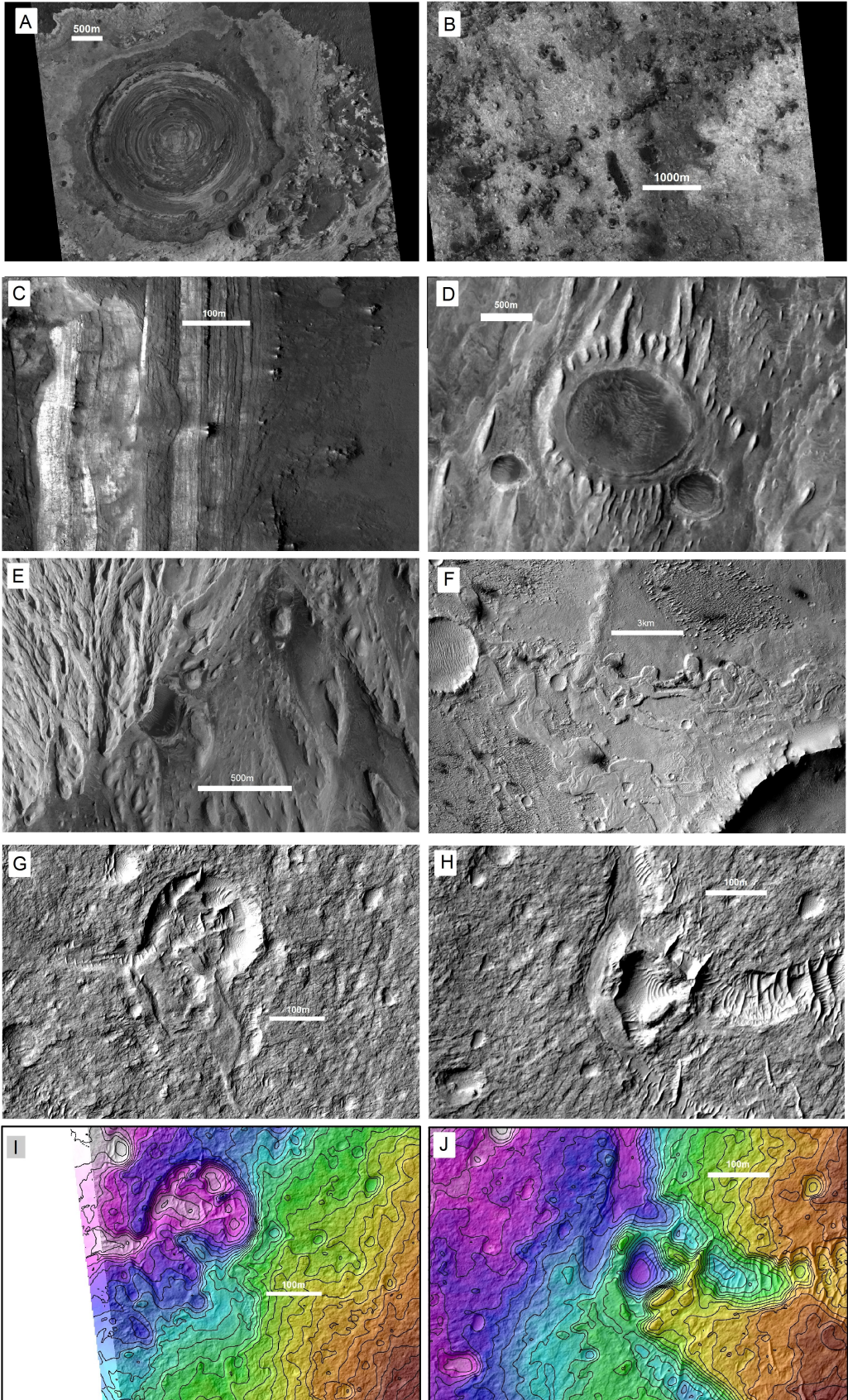
325 Werner, S.C. & Tanaka, K.L., 2011, Redefinition of the crater-density and absolute-age  
326 boundaries for the chronostratigraphic system of Mars. *Icarus*, 215, 603-607.

327 Wordsworth, R., et al., Global modelling of the early Martian climate under a denser CO<sub>2</sub>  
328 atmosphere, astro-ph:EP, arXiv:1207.3993.

329 Yen, A.S., et al., 2006, Nickel on Mars: Constraints on meteoritic material at the surface. *J.*  
330 *Geophys. Res.*, 111, E12S11.

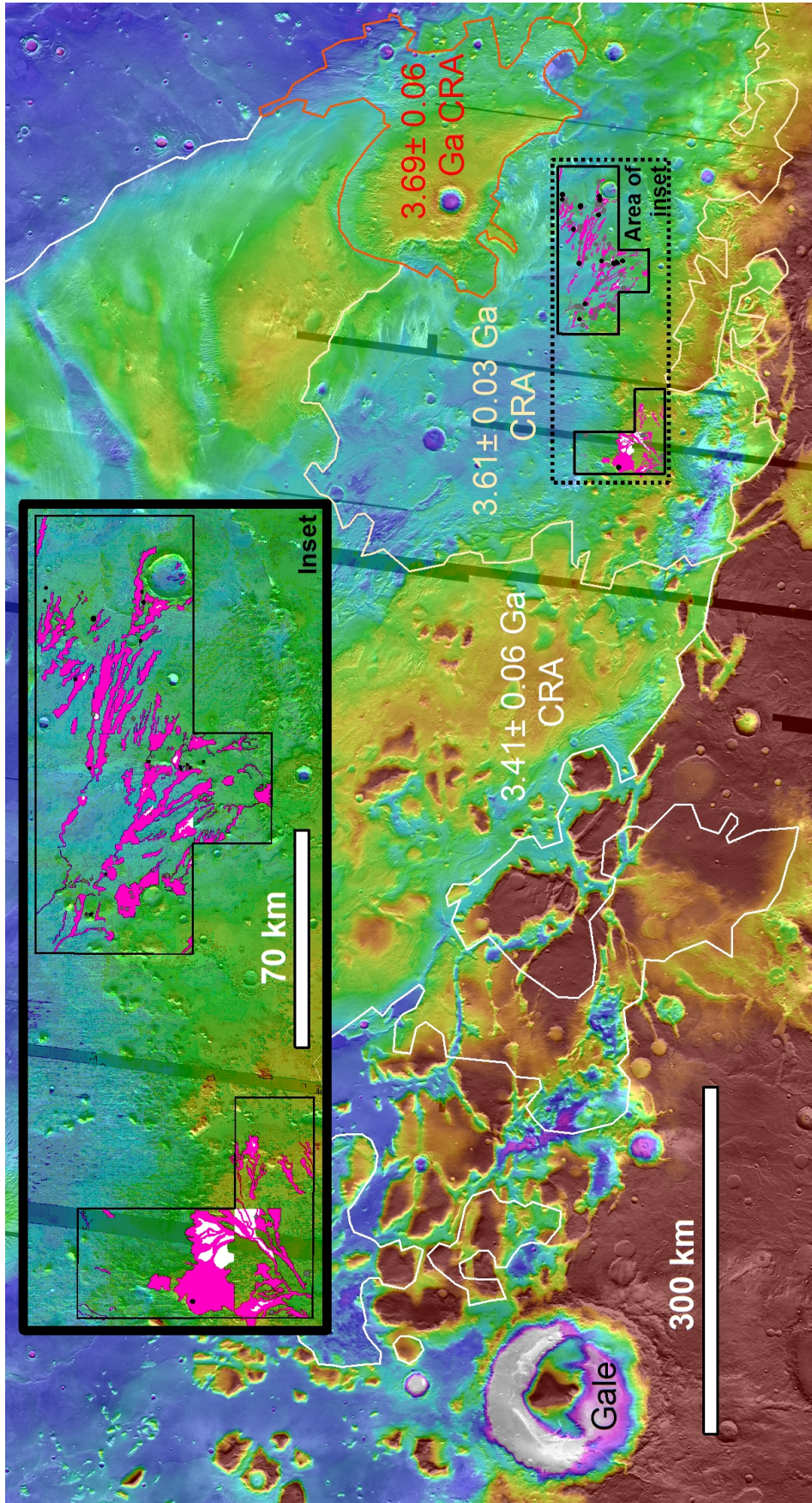
331 Yielding, G., et al., 1996, Sampling of fault populations using sub-surface data: a review, *J.*  
332 *Struct. Geol.*, 18,135-146.

333 Zimbelman, J.R., & Scheidt, S.P., 2012, Hesperian age for Western Medusae Fossae Formation,  
334 *Mars. Science* 336, 1683.

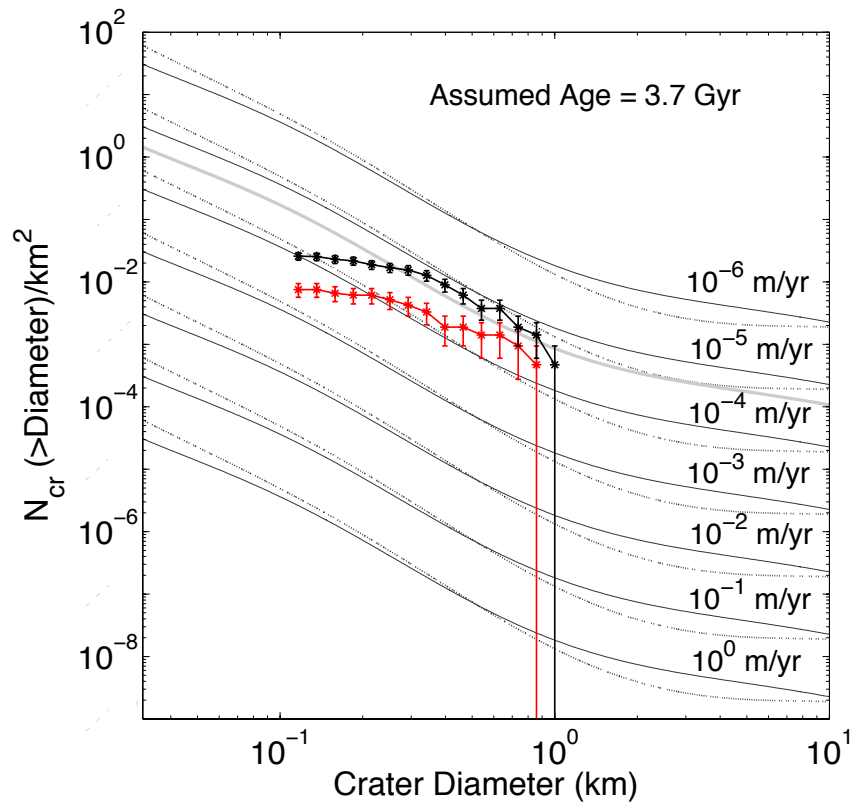


336 **Figure 1.** Varying styles of small-crater preservation on Mars. a) Concentric sediment fill of  
337 ~2km-diameter crater, Meridiani. PSP\_001981\_1825. See Edgett, (2005). b) Secondary-crater  
338 chain preserved as rimmed mesas, near Oyama Crater. Rimmed mesas are ~150m diameter.  
339 PSP\_010882\_2040. c) Buried impact exposed in cross-section by sidewall of later crater. Crater  
340 is ~200m across. ESP\_019664\_2035 d) Preservation in inverted relief of crater within Gale  
341 Crater's mound (Aeolis Mons). Crater is ~1.2 km across. G05\_020054\_1749\_XN\_05S222W. See  
342 Thomson et al. (2011). e) Crater being exhumed from beneath the lower unit/upper unit  
343 unconformity within Gale Crater's mound (Aeolis Mons). ESP\_019988\_1750. See Thomson et  
344 al. (2011). f) Craters with fresh-appearing ejecta being exhumed from beneath meander belts,  
345 Aeolis Dorsa, P15\_006973\_1742\_XI\_05S205W; Burr et al., 2010. g) Crater being exhumed from  
346 beneath fluvial channel deposit, Aeolis Dorsa. #6 in Supplementary Table, 238 m diameter.  
347 ESP\_019104\_1740. h) Crater draped by fluvial channel deposit, Aeolis Dorsa,  
348 ESP\_019104\_1740. #3 in Supplementary Table, 141 m diameter. i) Crater from (g), but with  
349 1m elevation contours from 1m DTM. DTM is composed of ESP\_019104\_1740 and  
350 ESP\_017548\_1740. j) Crater from (h), with 1m contours from same DTM.



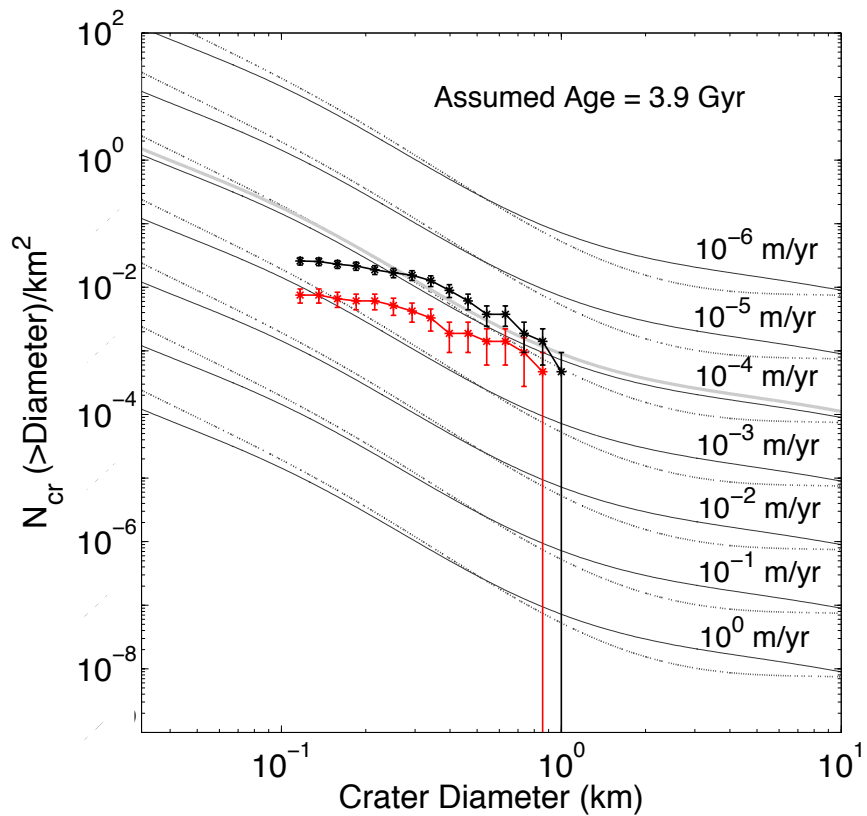


352 **Figure 2.** Location of study area (black polygons outlining bright pink areas) in relation to Gale  
353 Crater and to areas with Crater-Retention Ages (CRAs) determined by Zimbelman & Scheidt  
354 (2012). Color scale corresponds to MOLA elevation, is linear, and saturates at -1000m (red)  
355 and -3500m (white). Red-outlined area is typically 500m higher than the fluvial-channel  
356 deposits. Gale’s lower mound accumulated at the same time, within error (Thomson et al.,  
357 2011). Inset shows zoom on count region. Within the count region, bright pink areas  
358 correspond to counted fluvial-channel deposits, black circles to embedded craters associated  
359 with those fluvial deposits, dark gray circles to possible embedded craters, and white areas to  
360 “holes” (areas not counted due to poor preservation) within fluvial-channel deposits. Circles  
361 representing craters are not to scale. Only a small subset of fluvial-channel deposits was used  
362 for this count (Burr et al., 2009).  
363



364

a)



365

366

b)

367 **Figure 3.** Aeolis Dorsa embedded-crater frequencies, plotted against sedimentation-rate  
368 curves for (a) assumed age 3.7 Ga and (b) assumed age 3.9 Ga. Red lines with symbols  
369 correspond to counts of definite river-crater interactions (Supplementary Table); Black lines  
370 with symbols correspond to counts including all candidates. Thin lines are lines of equal  
371 sedimentation rate using crater production functions and chronology functions given by  
372 Werner & Tanaka, 2011. Thin dotted lines employ “Ivanov” crater production function and  
373 “Hartmann & Neukum” chronology function. Thin solid lines employ “Hartmann” crater  
374 production function and “Hartmann 2005” chronology function. All function parameters are  
375 taken from Werner & Tanaka (2011). Thick gray line corresponds to best-fitting accumulation  
376 rate.